Published in final edited form as:
Biomaterials. 2012 November ; 33(33): 8329–8342. doi:10.1016/j.biomaterials.2012.08.013.

Bone scaffold architecture modulates the development of mineralized bone matrix by human embryonic stem cells

Ivan Marcos-Campos[1], **Darja Marolt**[1,3], **Petros Petridis**[1], **Sarindr Bhumiratana**[1], **Daniel Schmidt**[2], and **Gordana Vunjak-Novakovic**[1]

[1]Department of Biomedical Engineering, Columbia University, New York NY 10032, USA

[2]Department of Plastics Engineering, University of Massachusetts Lowell, Lowell MA 01854, USA

Abstract

Decellularized bone has been widely used as a scaffold for bone formation, due to its similarity to the native bone matrix and excellent osteoinductive and biomechanical properties. We have previously shown that human mesenchymal and embryonic stem cells form functional bone matrix on such scaffolds, without the use of growth factors. In this study, we focused on differences in bone matrix that exist even among identical harvesting sites, and the effects of the matrix architecture and mineral content on bone formation by human embryonic stem cells (hESC). Mesenchymal progenitors derived from hESCs were cultured for 5 weeks in decellularized bone scaffolds with three different densities: low (0.281 ± 0.018 mg/mm^3), medium (0.434 ± 0.015 mg/mm^3) and high (0.618 ± 0.027 mg/mm^3). The medium-density group yielded highest densities of cells and newly assembled bone matrix, presumably due to the best balance between the transport of nutrients and metabolites to and from the cells, space for cell infiltration, surface for cell attachment and the mechanical strength of the scaffolds, all of which depend on the scaffold density. Bone mineral was beneficial for the higher expression of bone markers in cultured cells and more robust accumulation of the new bone matrix.

Keywords

tissue engineering; decellularized scaffold; bone; human embryonic stem cells; mineralization

1. Introduction

An increasing number of patients suffer from osteochondral defects that require transplantation [1]. Bone autografts [2], the gold standard for replacing large regions of damaged bone, are limited by donor site morbidity and the volume of bone that can be harvested [3, 4]. Other reported strategies such as allogenic transplants are limited by the risk of rejection [5]. Bone tissue engineering is a promising alternative method, in which autologous cells are combined with supporting biodegradable material scaffolds, or cultured

Please address correspondence to: Gordana Vunjak-Novakovic, Mikati Foundation Professor of Biomedical Engineering and Medicine, Columbia University, Department of Biomedical Engineering, Vanderbilt Clinic 12th floor, Room 12-234, 622 W 168th Street, New York NY 10032, tel. 212-305-2304; fax: 212-305-4692, gv2131@columbia.edu.
[3]Present address: The New York Stem Cell Foundation, New York, NY 10032

Conflict of Interest: Authors declare no conflict of interest.

in bioreactors to generate biological bone substitutes [6]. At the same time, engineered bone tissue is an invaluable model for quantitative studies of bone development, remodeling and disease, as it provides biologically meaningful system in which the environmental parameters can be systematically varied and controlled.

Bone tissue engineering studies have mostly utilized human mesenchymal stem cells (hMSC) isolated from bone marrow aspirates and expanded in culture [7, 8]. However, the formation of normal healthy bone require multiple cells types - osteoblasts, osteoclasts, vascular and nerve cells, that act in concert to maintain bone structure and function [9]. Pluripotent hESC, but not hMSCs, can give rise to all these different cell lineages residing in bone, and are therefore an ideal biological model to study bone development. Studies of hESCs also form a basis for the use of induced pluripotent stem cells (iPSC) that can be derived for autologous use in regenerative medicine, and to study normal and pathological bone function in cells from a large pool of patients[10–12]

Prior work established the feasibility of hESC differentiation into mesenchymal cells [13–15] osteoblasts [16–18], chondrocytes [19, 20], endothelial [21] and neural cells [22]. hESCs-derived mesenchymal progenitors (MP) were shown to share many features with the adult hMSCs derived from bone marrow [23]. Detailed microarray comparison of hESC-MP and hMSC showed extensive similarities [24] and indicated that hESC-MPs derived mesenchymal progenitors display higher proliferation potential and matrix mineralization potential compared to *in vitro* expanded BMSC.

Different types of materials have been utilized to engineer bone *in vitro* and implant it *in vivo*, including polymeric materials [25, 26], ceramic [27], silk protein with or without incorporated mineral phase [28–31], and decellularized native bone [32, 33]. While synthetic materials offer control over scaffold properties including composition, structural and mechanical properties, native bone scaffolds offer the advantages of the microenvironment and mechanical properties found in vivo, including composition and native tissue structure. Native bone may also be partially and fully demineralized to enable osteogenic molecules previously embedded in the matrix to become exposed and interact with seeded cells [34, 35], enhancing bone formation [33].

Internal architecture of the scaffold directly determines the cellular microenvironment, and affects the cell growth, signaling and osteogenic differentiation depending on the cell type [36]. Scaffold porosity determines the available space for cells to proliferate and assemble the new tissue matrix. Pore size affects cell migration and infiltration within the scaffold [37, 38]. It has been shown that the pore size and porosity determine the seeding efficiency and subsequent proliferation of both the mesenchymal stem cells [39] and the embryonic stem cells [40, 41], presumably due to the effects on available internal surface area. As the porosity increases, so does the total void volume. In parallel with the reduced amount of scaffold material per unit volume the mechanical properties decrease, resulting in a lower strength of the scaffolds [42]).

In our previous work, we optimized tissue engineering of bone in perfusion bioreactors using decellularized bovine bone [32, 43–45]. Decellularized native bone of selected density provided excellent structural and mechanical support for bone formation by the seeded hMSCs and hESCs, and exhibited osteogenic features that were strong enough to grow the bone *in vitro* without supplementing bone morphogenetic proteins [32, 45]. Bone grafts engineered *in vitro* from hESCs contained dense bone matrix that further matured over eight weeks of subcutaneous implantation and connected to the host vasculature, showing signs of remodeling, without a single incidence of teratoma [45]

However, significant differences exist in native bone density and architecture depending on the harvesting site and little is known how these affect the growth and osteogenesis of hESC-MP. Therefore the aim of the present study was to systematically evaluate the properties of decellularized bovine bone scaffolds sorted by density, and evaluate the effects of different bone density groups on osteogenesis and bone tissue formation by hESC-MP.

2. Materials and methods

2.1 Derivation of mesodermal progenitors from hESCs

Human embryonic stem cells (line H9 from WiCell Research Institute, Madison, WI) were plated on irradiated MEF feeder layers and cultured in embryonic medium (KnockOut DMEM supplemented with 20% KnockOut Serum Replacement, 1 mM L-glutamine, 1% penicillin/streptomycin, 0.1 mM non essential amino acids, 0.1 mM mercaptoethanol and 5 ng/ml bFGF). Cells were incubated at 37°C with 5% CO_2 and passaged every 3–4 days. Medium was changed every day. Once confluence was reached, hESC colonies were switched to mesodermal medium (KnockOut DMEM supplemented with 20% Hyclone FBS and 1% penicillin/streptomycin) for 1 week to induce differentiation into mesodermal progenitors. After this time, cells were trypsinized and seeded on T150 flasks treated with 0.1% gelatin (1×10^5 cells/cm^2) and cultured in mesodermal medium (passage 0). Mesodermal progenitors were passaged when 80–90% confluence was reached, until the 5^{th} passage was reached that was used for the experiments. Medium was changed every 3–4 days.

2.2 Phenotypic characterization of mesodermal progenitors

Mesodermal progenitors (passage 5) were harvested and labeled with fluorochrome conjugated antibodies anti-SSEA1-Alexa Fluor® 488, anti-SSEA4-Alexa Fluor® 488, anti-CD44-FITC, anti-CD73-PE, anti-CD90-FITC, anti-CD166-PE, anti-CD31-Alexa Fluor® 488, anti- CD34-APC and anti-CD271-APC (BD Biosciences, Franklin Lakes, NJ). Unstained cells were used as a negative control. Following staining, cells were washed and then resuspended in flow cytometry buffer (PBS with 2 mM EDTA) prior to analysis in FACSCalibur flow cytometer (BD Biosciences, San Jose, CA, USA). The fraction of positive cells for each antibody was quantified using the FlowJo software version 7.6 (Tree Star Inc., Ashland, OR, USA).

2.3 Analysis of mesodermal progenitors multipotency

Monolayer differentiation—Mesodermal progenitors (passage 5) were plated in 24 well plates (1×10^4 cells/cm^2) and cultured for 4 weeks in either *control medium* (DMEM supplemented with 10% Hyclone FBS and 1% penicillin/streptomycin), or *osteogenic medium* (control medium supplemented with 1 μM dexamethasone, 10 mM β-glycerophosphate, 50 μM ascorbic acid-2-phosphate). At weeks 1, 2, 3 and 4, osteogenic differentiation was assessed by alkaline phosphatase activity (blue staining) (Sigma-Aldrich, St Louis, MO, USA), following the manufacturer's instructions.

Micromass differentiation—Mesodermal progenitors (3×10^5 cells) at passage 5 were centrifuged in 2 mL tubes and cultured for 4 weeks in *control medium* (DMEM supplemented with 10% Hyclone FBS and 1% Pen/Strep), *osteogenic medium* (control medium, supplemented with 1 μM dexamethasone, 10 mM β-glycerophosphate, 50 μM ascorbic acid-2-phosphate) and *chondrogenic medium* (DMEM supplemented with 1% PenStrep, 100 nM dexamethasone, 50 μg/ml ascorbic acid-2- phosphate, 40 μg/ml L-proline, 1 × ITS, 1 mM sodium pyruvate, 10 ng/ml tumor growth factor β-3). After 4 weeks, the cells were fixed in 10% formalin for 24 hours, dehydrated and embedded in paraffin for histological staining. Mineralization was assessed by von Kossa staining. Sections were

incubated with 1% $AgNO_3$ solution in water and exposed to a 60 W light for 1 hour, to develop a black stain indicative of phosphate deposits. Chondrogenic differentiation was assessed by Alcian Blue staining of deposited glycoaminoglycans. Histological stains were documented using a light microscope (Olympus IX81 light microscope, Center Valley, PA).

2.4 Bone scaffold preparation

Trabecular bone was harvested from bovine wrists (Green Village Packing) as in our previous studies [44, 45]. Wrists were drilled longitudinally through the center of the bone shaft starting from the superior end of the forelimb. The cores were incubated in a series of solutions until fully decellularized: (1) PBS + 0.1% EDTA for one hour, (2) 10mM Tris + 0.1% EDTA for 12 hours at 11°C while shaking, (3) 0.5% SDS + Tris 10mM for 24 hours. After washing with PBS, remaining biological components were then removed by treatment with DNAse and RNAse (100 U/ml) for 6 hours at 37°C. The cores were washed twice more with PBS and ethanol, and lyophilized. Cylindrical-shaped scaffolds (4 mm in diameter by 2 mm in thickness) were prepared and measured for determination of exact volume with caliper. Scaffolds were weighed, density was calculated and the scaffolds were sorted into three experimental groups according to density: low (0.281 ± 0.018 mg/mm^3), medium (0.434 ± 0.015 mg/mm^3) and high (0.618 ± 0.027 mg/mm^3).

For the assessment of the influence of native bone matrix composition on osteogenic differentiation, medium density scaffolds were fully demineralized by incubation in 0.6N HCl for 4 hours at room temperature. Following demineralization, scaffolds were extensively rinsed in distilled water and sterilized with ethanol.

2.5 Scaffold characterization

Pore size and surface area were measured using a PoreMaster 33 mercury intrusion porosimeter (Quantachrome Instruments, Boynton Beach, FL, USA). Scaffolds were placed in a glass penetrometer (0.5 cm^3 stem volume) which was sealed and evacuated to a pressure of less than 50 millitorr, then pressurized with mercury to 50 psi, then depressurized to 0.2 psi, to generate a complete intrusion-extrusion cycle covering a pore size range of ~4 μm to ~1 mm. Three scaffolds from the same density class were used for each analysis (representing a total sample between ~40 and ~100 mg, with the results reflecting an average over those three. Four such analyses were performed per density class to generate reliable statistics. Pore size was determined mathematically by the Washburn equation [46]:

$$P_c = \frac{2\gamma}{r}\cos\theta \quad (1)$$

where P_c is the capillary pressure, γ is the surface tension of the mercury within the capillary, r is the radius of the pore and θ is the contact angle between the mercury and the pore wall (θ = 140°). The surface area of all pores and voids filled up to a pressure P was calculated using the formula of Rootare and Prenzlow [47]:

$$S = \frac{1}{\gamma|\cos\theta|}\int_0^V P\,dV \quad (2)$$

All of the above calculations were performed automatically using the Quantachrome Poremaster for Windows 5.10 software package.

The relative volume fraction of trabecular bone (BV) in the scaffolds was determined by μCT (see below), and used to calculate the scaffold porosity (P):

$$P=(1-BV)\times 100 \quad (3)$$

Mechanical properties of four scaffolds from each group were determined by measuring the elastic modulus using a mechanical testing machine. We used an initial tare load of 0.1 N that was followed by periods of stress and relaxation intervals where the unseeded scaffolds were compressed to 10% strain at a ramp velocity of 0.5%/s and maintained at that position for 1,800 sec. Equilibrium forces measured at 10% strain were used to calculate Young's modulus.

2.6 Cell seeding and culture on bone scaffolds

Mesodermal progenitors (passage 5) were resuspended in osteogenic medium (3×10^8 cells/ml). 20 μl (containing 6×10^5 cells) of cell suspension were seeded into the bone scaffolds from all experimental groups (low density, medium density, medium density demineralized, and high-density). Scaffolds were flipped every fifteen minutes for one hour to achieve uniform cell distribution. Osteogenic medium (6 ml per well) were added, and seeded scaffolds were cultured at 37°C in a humidified atmosphere of 5% CO_2. Media was changed every 3–4 days.

2.7 Live-Dead assay

At timed intervals, constructs were harvested and cut in half. One half of each scaffold was incubated in RPMI phenol-free medium with calcein (staining for live cells) and ethidium homodimer-1 (staining for dead cells) for 45 min in the dark, as indicated by the manufacturer's protocol (LIVE/DEAD® Viability/Cytotoxicity Kit, Molecular Probes). The central and edge regions of each sample were imaged with a fluorescence microscope (Olympus IX81 light microscope, Center Valley PA).

2.8 DNA assay

Constructs were cut in half (n=4 per group), washed in PBS and incubated overnight with 1 mL of digestion buffer (10 mM Tris, 1 mM EDTA, 0.1% Triton X-100 and 0.1 mg/mL proteinase K) at 50°C. Supernatants were collected and diluted 10 times, and DNA was quantified using the Picogreen assay (Invitrogen), following the manufacturer's instructions. A standard curve was prepared from a solution of lambda DNA (Molecular Probes). Samples were read using a fluorescent plate reader at an excitation wavelength of 480nm and an emission wavelength of 528 nm.

2.9 Histology and immunohistochemistry

At times intervals, constructs (n=4) were harvested and cut in half. One half of each sample was fixed in 10% formalin for 24 hours and then decalcified with Immunocal (Decal Chemical Corp., Tallman, NY) for 2 days. Samples were dehydrated with graded ethanol washes, embedded in paraffin and serial longitudinal sections, 5 μm thick, were prepared for histology. Immunohistochemistry stainings were performed with specific primary antibodies and developed using the Vector Elite ABC kit (Vector Laboratories), following manufacturer instructions. Briefly, sections were blocked with serum for 30 min and then incubated with the primary antibody anti-osteopontin (1:500), anti-bone sialoprotein (1:500) or anti-osteocalcin (1:500) (all purchased from Millipore, Billerica, MA) overnight at 4°C. After washing with PBS, samples were incubated with secondary antibodies and developed (Vector Laboratories). Negative controls were prepared by omitting the primary antibody step.

Semi-quantitative analysis of the staining was conducted using ImageJ software version 1.44o (National Institutes of Health, USA). For bone marker stains, each image was converted to an RGB Stack and the green stack was used. Thresholding was performed using a value of 121 (selected based on the intensity of the negatively stained controls). Areas of new tissue were manually selected, and the fractional areas stained positively were measured for 4 samples (half scaffold each).

2.10 Gene expression analysis

Tissue constructs were harvested after 3 days, 1 week, 3 weeks, and 5 weeks of culture to evaluate the RNA levels of bone matrix proteins. Constructs were disintegrated in 1 mL of Trizol using steel beads and a bead beater rotator MiniBeadBeater-8 (Biospec Products, Bartlesville, OK). RNA was extracted using Trizol reagent according to the manufacturer's instructions. cDNA was prepared from 1 μg of total mRNA using random hexamers and SuperScript First-Strand Synthesis System (Invitrogen). Osteopontin (OPN, Hs00167093_m1), bone sialoprotein (BSP, Hs00173720_m1), type I collagen (Col1, Hs01076780_g1), and glyceraldehyde-3-phosphate-dehydrogenase (GAPDH) assay on demands were purchased from Applied Biosystems (Foster City, CA, USA). Real-time PCR was performed on the ABI Prism 7700 Sequence Detection Instrument (Applied Biosystems, Foster City, CA, USA). Expression of the bone specific genes was normalized to GAPDH and presented as relative values.

2.11 Microcomputerized tomography (μCT)

μCT was performed using a modification of a previously developed protocol [48] on scaffolds before culture and cultured constructs. After fixation with glutaraldehyde, the samples were aligned along their axial direction and stabilized with wet gauze in a 15mL centrifuge tube that was clamped in the specimen holder of a vivaCT 40 system (SCANCO Medical AG, Basserdorf, Switzerland). The 4 mm length of the scaffold was scanned at an isotropic resolution of 21 μm. The total bone volume (BV), which consists of the bone matrix in the scaffold and the new mineralized bone, bone volume relative to total volume (BV/TV), trabecular number (Tb.N.), trabecular thickness (Tb.Th.) and intertrabecular space (Tb.Sp.) were obtained from the application of a global thresholding technique so that only the mineralized tissue is detected. Spatial resolution of this full voxel model was considered sufficient for evaluating the microarchitecture of the samples.

2.12 Statistical analysis

Paired t-test and Multiway Analysis of Variance (ANOVA) were used to analyze significant differences between the groups at the same time point, and within the group at different time points, followed by Tukey's post hoc analysis using PRISM software, with $p < 0.05$ being considered as statistically significant.

3. Results

3.1 Properties of decellularized trabecular bone scaffolds

Decellularized bovine trabecular bone scaffolds were sorted according to their density into three experimental groups, characterized and tested for growing engineered bone from hESC-derived mesenchymal progenitors (Fig. 1). Mercury intrusion porosimetry measurements indicated a significant increase in internal surface area with increasing scaffold density (Fig. 2), from 1.3 ± 0.2 cm^2 for low-density scaffolds, to 4.2 ± 2.0 for medium-density scaffolds, and 7.7 ± 2.6 cm^2 for high-density scaffolds. In parallel, the pore size decreased from 376 ± 21 μm in low-density scaffolds, to 315 ± 17 μm in medium density scaffolds, and 208 ± 27 μm in high-density scaffolds. Bone scaffold porosity decreased with increasing scaffold density, from 88.3 ± 1.0% for low-density scaffolds to

80.4 ± 1.7% for medium-density scaffolds and 70.4 ± 1.5% for high-density scaffolds. Mechanical properties of the scaffolds markedly improved with the increasing scaffold density, with the compressive elastic modulus of 15 ± 4 MPa for low-density scaffolds, to 45 ± 7.7 MPa for medium density scaffolds and 55 ± 3.3 MPa for high density scaffolds (Fig. 2).

3.2 Properties of hESC-derived mesodermal progenitors

Analysis of cell surface markers by flow cytometry revealed that the majority of mesodermal progenitors derived from hESC and expanded to passage 5 expressed mesenchymal surface molecules CD44, CD71, CD90 and CD166. Notably, specific markers of embryonic stem cells (SSEA-1 and SSEA-4), hematopoietic cells (CD34) endothelial cells (CD31) and neural cells (CD271) were not expressed (Fig. 3a). Mesodermal progenitors cultured under osteogenic conditions for 4 weeks expressed alkaline phosphatase activity in monolayers, an early marker of osteogenesis (Fig. 3b), and von Kossa staining in micromass cultures, an indicator of matrix mineralization (Fig. 3c). Alcian blue staining of micromass cultures showed higher GAG accumulation for chondrogenic medium as compared to control medium (Fig. 3c).

3.3 Viability and growth of hESC-mesenchymal progenitors in bone scaffolds

The internal bone scaffold architecture had profound effects on cell proliferation and density. Live/Dead analysis revealed uniform distribution of cells throughout the scaffolds at all time points, and demonstrated that most of the cells were viable after 5 weeks of culture with no apparent changes over time, regardless of the experimental group (Fig. 4a). H&E staining of cultured scaffolds revealed uniform cell distribution after 3 days of culture, with thin cell layers lining the scaffold surfaces. Over the first week of culture, cell density was relatively constant in all groups (Fig. 4b). However after additional 2 weeks of culture, the cell numbers increased, and the majority of the internal spaces in low- and medium-density scaffolds were filled with cells, in contrast to high-density scaffolds which exhibited areas in the scaffold interior devoid of cells. These cell distributions were maintained throughout the culture. In all groups, areas with the greatest cell density were observed close to the scaffold surfaces (Fig. 4b).

Histological analyses were corroborated by the biochemical analysis of the DNA content in the cultured constructs (Fig. 4c). On day 1 after the scaffold seeding, we observed somewhat lower DNA content in low-density scaffolds as compared to medium-density and high-density scaffolds. After 3 weeks of culture, a 7.2-fold and 4.5-fold increase in DNA content was observed in low- and medium-density scaffolds, respectively, whereas the DNA contents increased only 2-fold in high-density scaffolds. These DNA contents were maintained through week 5 of culture, suggesting that the final cell density was reached by 3 weeks of culture.

3.4 Effect of bone scaffold on osteogenic gene expression

Osteogenic differentiation of the hESC-progenitors cultured in bone scaffolds was evaluated by the real time analysis of gene expression of bone markers (Fig. 5). The expression levels of collagen type I were highest on day 3 of culture, and significantly higher in high density than either low or medium density groups. The expression levels of osteopontin (OPN) also increased with scaffold density at day 3 and week 1 of culture, and decreased with time. In contrast, the expression of bone sialoprotein (BSP) was detected only after 3 weeks of culture and further increased through week 5 in all experimental groups, demonstrating the progression of osteogenic differentiation. By week 5 of culture, no significant differences were found between the groups in gene expression profiles of the evaluated bone markers.

3.5 Effects of bone scaffold density on bone matrix deposition and mineralization

Development of bone specific matrix was confirmed by positive immunohistochemical staining of bone proteins OPN, BSP and OCN. The constructs from all groups showed an increase in staining over time, from week 1 to week 5 of culture (Fig. 6). The areas staining strongly for bone proteins co-localized with the areas of high cell density, positioned along the outer surfaces of the constructs, and were not significantly different in intensity for scaffolds of different densities. After 5 weeks of culture, the inner regions of the medium-density bone scaffolds exhibited significantly higher staining of OPN and BSP compared to other groups, suggesting that the density of bone scaffolds significantly affects bone matrix development (Fig. 7).

Bone formation was also evaluated by μCT scans of bone constructs before and after 5 weeks of culture. Mineralized tissue formation was observed in scaffolds of all density groups (Fig. 8a). Bone volume (BV) (Fig. 8b) and bone volume to tissue volume ratio (BV/TV) (Fig. 8c) increased significantly in medium- and high-density groups compared to the initial scaffolds. The increases in BV and BV/TV ratio were the highest in medium-density group, consistent with the strongest presence of bone proteins in this group. The trabecular thickness (Tb.Th.) (Fig. 8f) had a trend of increase, and the inter-trabecular space (Tb.Sp.) (Fig. 8e) had a trend of decrease, but without statistically significant differences compared to initial scaffolds. No significant increases in trabecular numbers (Tb.N.) (Fig. 8d) were found in any of the groups over week 5 of culture.

3.6 Effect of bone scaffold mineralization on bone tissue deposition and mineralization by hESC-derived mesodermal progenitors

Scaffolds in the medium–density range were demineralized to assess the influence of the matrix composition on osteogenic differentiation. Demineralization had no significant effects on final DNA contents (Fig. 9a), cell viability and distribution (Fig. 9b), and the expression of osteogenic genes that followed the characteristic bone formation pattern in both groups (Fig. 9c). Somewhat higher staining of OPN was observed in the inner regions of mineralized scaffolds as compared to demineralized scaffolds, but no differences were found in BSP and type I collagen staining (Fig. 9d–e). Quantification of morphological parameters obtained by μCT confirmed new bone formation in both mineralized and demineralized scaffolds. The relative amount of new bone formation was much higher in mineralized scaffolds, and the increase of trabecular number and thickness was higher in demineralized scaffolds (Fig. 9f).

4. Discussion

Bone tissue engineering, using osteogenic cells and scaffolds, is making major strides towards generating viable and functional substitutes of native bone, and enabling controlled studies of bone development and modeling under biologically sound conditions. We previously showed that scaffolds made by decellularizing native bone support the formation of engineered bone by both human mesenchymal stem cells [32] and human embryonic stem cells [45], to the extent that the supplementation of BMPs was not necessary. In all studies, the native bone used as a scaffold provided a favorable combination of appropriate composition, structure, and biomechanics, and exhibited strong osteogenic properties. Because these properties vary quite significantly in native bone, there are also great variations in the properties of decellularized bone scaffolds. We therefore investigated the effects of internal scaffold architecture and the amount of mineral on bone formation by hESC-derived mesenchymal progenitors cultured *in vitro* for 5 weeks (Fig. 1). Consistent with previous reports for synthetic materials [49], the internal architecture of decellularized

bone scaffolds played a major role in osteogenic cell differentiation and matrix assembly in engineered bone constructs.

Overall, there appears to be a balance between the free space for cell infiltration, transport of nutrients and metabolites to and from the cells and the space for deposition of bone matrix (all of which are highest in low density scaffolds), and the size of internal surface area providing osteogenic factors and the mechanical strength of the scaffolds (both of which are highest in high density scaffolds) (Fig. 2). Among the three scaffold groups studied, the bone constructs engineered using medium-density scaffolds had the highest concentrations of live cells (Fig. 4) and tissue matrix (Fig. 6), in particular in the inner regions of the bone constructs (Fig. 7).

Consistent with the data previously reported [13, 45], hESCs were successfully induced to give rise to stable mesenchymal progenitors that were similar to hMSCs derived from adult bone marrow with respect to the expression of cell surface markers (Fig. 3a) [50]. Importantly, specific markers of embryonic stem cells (SSEA-4), hematopoietic cells (CD34) endothelial cells (CD31) and neural cells (CD271) were not expressed. These mesenchymal progenitors showed a mesenchymal-like phenotype and expressed markers of osteogenesis and chondrogenesis when cultured in monolayer and micromass under appropriate culture media stimulation (Fig. 3b,c).

The present study shows for the first time an internal architecture-dependent pattern of bone matrix development from hESC mesenchymal progenitors. Initially, cells in all density groups attached to all available internal surface areas. By week 3 cell distribution and proliferation becomes different between the groups (Fig. 4), with markedly higher densities of cells (Fig. 4b) in the low and medium density scaffold groups, presumably due to the favorable combination of sufficient surface area for cell attachment and large pores allowing cell infiltration, growth and transport of oxygen and nutrients. Comparable final cell densities found in low- and medium-density scaffold groups after 5 weeks of culture (Fig. 4b) suggest that actual cell concentration/void volume is higher in medium-density group due to the lower void volume (Fig. 2), enhancing cell-cell interaction and consequently bone matrix production [51]. In scaffolds of this size (diffusional distance of 1 mm), transport of oxygen and nutrients does not appear to be a limiting factor. For larger scaffolds, perfusion flow of medium through the cell-seeded scaffolds will be required to maintain cell viability in the interior region of the scaffolds, as we have shown in numerous previous studies, including those with hMSCs [43] and hESC-MPs [45] cultured on decellularized bone scaffolds.

The analysis of mRNA expression confirmed the progression of osteogenic differentiation (Fig. 5). Gene expression in osteogenic differentiation from hESC mesenchymal progenitors can be divided in two stages. Genes involved in cell proliferation, migration and ECM synthesis are present at the earlier stages, whereas those genes playing a role in maturation and mineralization are expressed at later stages of bone matrix formation [52]. Osteopontin, one of the genes encoding for a protein needed at early stages, reaches a peak at day 3, supporting cell-cell interactions [53] and migration [54]. According to this role in cell-cell and cell-matrix interactions, our data shows significant differences in OPN expression at day 3 between the density groups, with significantly higher expression in scaffolds with the highest numbers of cells at this time. As OPN was down-regulated during the following weeks, genes involved in mineralization and maturation, such as bone sialoprotein [55, 56], increase their expression demonstrating a phenotype maturation into osteoblast lineage. Transcript levels of type I collagen, the major constituent of the native bone matrix [57], were down-regulated after the first 3 days of culture, which is in agreement with previous

studies that reported higher synthesis of collagen at earlier stages of bone matrix formation [58, 59].

As expected, our data reveal strong relations between cell density and the accumulation of bone matrix proteins, including OPN, OCN and BSP. The outer regions of the scaffolds, populated with a higher number of cells, showed the strongest presence of all markers (Fig. 6, Fig. 7), without major differences between the groups (Fig. 7, bottom panels). In contrast, significant differences were found in the inner regions of the tissue constructs for all measured proteins, where medium-density group showed the strongest staining of OPN, OCN and BSP as compared to low- and high-density groups (Fig. 7, top panels). Unlike high-density-scaffolds, where void areas are found in at the centers of the constructs, presumably due to the diffusional limitations of oxygen transport, in medium-density scaffolds cells were present throughout the scaffold volumes, enhancing uniform matrix formation.

Deposition of mineralized matrix was clearly evident by μCT in all experimental groups (Fig. 8), with the highest increases in the absolute and relative volumes of mineralized matrix in the medium-density group (Fig. 8b,c). Interestingly, the new bone formation occurred through thickening of preexisting trabecular rather than through an increase in the number of trabeculae (Fig. 8e,f).

As previously seen for bone formation by hMSC in synthetic silk-mineral scaffolds [28], osteogenesis is highly dependent on the pre-existing amount of mineral in the matrix (Fig. 9). In contrast, a prior study by Mauney and colleagues showed that demineralized native bone scaffolds enhanced bone formation by hMSC [60]. Demineralization method used in their study was different from our current study, and we hypothesize that the overall cellular responses could be affected by different access to osteoinductive molecules embedded in the matrix, in particular in the inner regions of the scaffolds. The complete removal of cellular material, associated with the preservation of tissue matrix proteins [32], enables the presentation of osteoinductive molecules modulating cell behavior. However, the mineral itself is highly osteoconductive as well, as shown in our recent study [28] in which we systematically varied the amount of mineral (hydroxyapatite) in silk scaffolds, thereby changing the osteoconductive and mechanical properties of the scaffolds. In this study, as well as our current work, the formation of bone-like structures and the increase in the equilibrium Young's modulus strongly correlated with the mineral content in the scaffolds. We identified two mechanisms by which the incorporated mineral enhanced the formation of tissue-engineered bone: through increased osteoconductivity of the scaffold, and by providing nucleation sites for the deposition and assembly of the new mineral. Consistent with these findings obtained from hMSCs, the present study also shows beneficial effects of bone mineral in the scaffold on the synthesis and assembly of mineralized bone tissue matrix by hESCs (Fig. 9).

5. Conclusion

We investigated the effects of the internal architecture of fully decellularized trabecular bone scaffolds on bone formation by hESC-derived mesenchymal progenitors cultured on scaffolds with low, medium and high bone matrix density. For the best scaffold group (medium density), we also evaluated the effects of matrix demineralization. The internal architecture of bone scaffolds had major role in the progression of osteogenic differentiation of mesenchymal progenitor cells derived from hESC, and in the assembly of engineered bone. The medium-density group yielded highest densities of cells and newly assembled bone matrix, presumably due to the best balance between the transport rates of nutrients and metabolites, space for cell infiltration, surface for cell attachment and the mechanical

strength, all of which depend on the scaffold density. Bone mineral was beneficial for the higher expression of bone markers in cultured cells and more robust accumulation of the new mineralized bone matrix.

Acknowledgments

We gratefully acknowledge funding support by the NIH (grants DE016525 and EB002520 to G.V.N.), the New York Stem Cell Foundation (Stanley and Fiona Druckenmiller fellowship to D.M., grant CU09-3055 to GVN), Slovenian Research Agency (grant P3-0371 to D.M.), the Aragón Government and Aragón Health Research Institute (fellowship to I.M.C.). We also thank Edward Guo for the use of μCT and Andrew Gerson for the use of Olympus microscopy room.

References

1. Vacanti JP, Langer R. Tissue engineering: the design and fabrication of living replacement devices for surgical reconstruction and transplantation. Lancet. 1999; 354(Suppl 1):SI32–4. [PubMed: 10437854]
2. Damien CJ, Parsons JR. Bone graft and bone graft substitutes: a review of current technology and applications. J Appl Biomater. 1991; 2:187–208. [PubMed: 10149083]
3. Brighton CT, Shaman P, Heppenstall RB, Esterhai JL Jr, Pollack SR, Friedenberg ZB. Tibial nonunion treated with direct current, capacitive coupling, or bone graft. Clin Orthop Relat Res. 1995:223–34. [PubMed: 7497673]
4. Goulet JA, Senunas LE, DeSilva GL, Greenfield ML. Autogenous iliac crest bone graft. Complications and functional assessment. Clin Orthop Relat Res. 1997:76–81. [PubMed: 9186204]
5. Kainer MA, Linden JV, Whaley DN, Holmes HT, Jarvis WR, Jernigan DB, et al. Clostridium infections associated with musculoskeletal-tissue allografts. N Engl J Med. 2004; 350:2564–71. [PubMed: 15201413]
6. Petite H, Viateau V, Bensaid W, Meunier A, de Pollak C, Bourguignon M, et al. Tissue-engineered bone regeneration. Nat Biotechnol. 2000; 18:959–63. [PubMed: 10973216]
7. Bruder SP, Jaiswal N, Haynesworth SE. Growth kinetics, self-renewal, and the osteogenic potential of purified human mesenchymal stem cells during extensive subcultivation and following cryopreservation. J Cell Biochem. 1997; 64:278–94. [PubMed: 9027588]
8. Meinel L, Karageorgiou V, Fajardo R, Snyder B, Shinde-Patil V, Zichner L, et al. Bone tissue engineering using human mesenchymal stem cells: effects of scaffold material and medium flow. Ann Biomed Eng. 2004; 32:112–22. [PubMed: 14964727]
9. Zaidi M. Skeletal remodeling in health and disease. Nat Med. 2007; 13:791–801. [PubMed: 17618270]
10. Bock C, Kiskinis E, Verstappen G, Gu H, Boulting G, Smith ZD, et al. Reference maps of human ES and iPS cell variation enable high-throughput characterization of pluripotent cell lines. Cell. 2011; 144:439–52. [PubMed: 21295703]
11. Takahashi K, Tanabe K, Ohnuki M, Narita M, Ichisaka T, Tomoda K, et al. Induction of pluripotent stem cells from adult human fibroblasts by defined factors. Cell. 2007; 131:861–72. [PubMed: 18035408]
12. Warren L, Manos PD, Ahfeldt T, Loh YH, Li H, Lau F, et al. Highly efficient reprogramming to pluripotency and directed differentiation of human cells with synthetic modified mRNA. Cell Stem Cell. 2010; 7:618–30. [PubMed: 20888316]
13. Barberi T, Willis LM, Socci ND, Studer L. Derivation of multipotent mesenchymal precursors from human embryonic stem cells. PLoS Med. 2005; 2:e161. [PubMed: 15971941]
14. Lian Q, Lye E, Suan Yeo K, Khia Way Tan E, Salto-Tellez M, Liu TM, et al. Derivation of clinically compliant MSCs from CD105+, CD24- differentiated human ESCs. Stem Cells. 2007; 25:425–36. [PubMed: 17053208]
15. Olivier EN, Rybicki AC, Bouhassira EE. Differentiation of human embryonic stem cells into bipotent mesenchymal stem cells. Stem Cells. 2006; 24:1914–22. [PubMed: 16644919]

16. Ahn SE, Kim S, Park KH, Moon SH, Lee HJ, Kim GJ, et al. Primary bone-derived cells induce osteogenic differentiation without exogenous factors in human embryonic stem cells. Biochem Biophys Res Commun. 2006; 340:403–8. [PubMed: 16389066]

17. Kuznetsov SA, Cherman N, Robey PG. In vivo bone formation by progeny of human embryonic stem cells. Stem Cells Dev. 2011; 20:269–87. [PubMed: 20590404]

18. Mateizel I, De Becker A, Van de Velde H, De Rycke M, Van Steirteghem A, Cornelissen R, et al. Efficient differentiation of human embryonic stem cells into a homogeneous population of osteoprogenitor-like cells. Reprod Biomed Online. 2008; 16:741–53. [PubMed: 18492382]

19. Hwang NS, Varghese S, Lee HJ, Zhang Z, Ye Z, Bae J, et al. In vivo commitment and functional tissue regeneration using human embryonic stem cell-derived mesenchymal cells. Proc Natl Acad Sci U S A. 2008; 105:20641–6. [PubMed: 19095799]

20. Oldershaw RA, Baxter MA, Lowe ET, Bates N, Grady LM, Soncin F, et al. Directed differentiation of human embryonic stem cells toward chondrocytes. Nat Biotechnol. 2010; 28:1187–94. [PubMed: 20967028]

21. James D, Nam HS, Seandel M, Nolan D, Janovitz T, Tomishima M, et al. Expansion and maintenance of human embryonic stem cell-derived endothelial cells by TGFbeta inhibition is Id1 dependent. Nat Biotechnol. 2010; 28:161–6. [PubMed: 20081865]

22. Lee H, Shamy GA, Elkabetz Y, Schofield CM, Harrsion NL, Panagiotakos G, et al. Directed differentiation and transplantation of human embryonic stem cell-derived motoneurons. Stem Cells. 2007; 25:1931–9. [PubMed: 17478583]

23. de Peppo GM, Sjovall P, Lenneras M, Strehl R, Hyllner J, Thomsen P, et al. Osteogenic potential of human mesenchymal stem cells and human embryonic stem cell-derived mesodermal progenitors: a tissue engineering perspective. Tissue Eng Part A. 2010; 16:3413–26. [PubMed: 20536357]

24. de Peppo GM, Svensson S, Lenneras M, Synnergren J, Stenberg J, Strehl R, et al. Human embryonic mesodermal progenitors highly resemble human mesenchymal stem cells and display high potential for tissue engineering applications. Tissue Eng Part A. 2010; 16:2161–82. [PubMed: 20136402]

25. Ishaug SL, Crane GM, Miller MJ, Yasko AW, Yaszemski MJ, Mikos AG. Bone formation by three-dimensional stromal osteoblast culture in biodegradable polymer scaffolds. J Biomed Mater Res. 1997; 36:17–28. [PubMed: 9212385]

26. Liu X, Ma PX. Polymeric scaffolds for bone tissue engineering. Ann Biomed Eng. 2004; 32:477–86. [PubMed: 15095822]

27. Grundel RE, Chapman MW, Yee T, Moore DC. Autogeneic bone marrow and porous biphasic calcium phosphate ceramic for segmental bone defects in the canine ulna. Clin Orthop Relat Res. 1991:244–58. [PubMed: 1850335]

28. Bhumiratana S, Grayson WL, Castaneda A, Rockwood DN, Gil ES, Kaplan DL, et al. Nucleation and growth of mineralized bone matrix on silk-hydroxyapatite composite scaffolds. Biomaterials. 2011; 32:2812–20. [PubMed: 21262535]

29. Marolt D, Augst A, Freed LE, Vepari C, Fajardo R, Patel N, et al. Bone and cartilage tissue constructs grown using human bone marrow stromal cells, silk scaffolds and rotating bioreactors. Biomaterials. 2006; 27:6138–49. [PubMed: 16895736]

30. Meinel L, Karageorgiou V, Hofmann S, Fajardo R, Snyder B, Li C, et al. Engineering bone-like tissue in vitro using human bone marrow stem cells and silk scaffolds. J Biomed Mater Res A. 2004; 71:25–34. [PubMed: 15316936]

31. Rockwood DN, Gil ES, Park SH, Kluge JA, Grayson W, Bhumiratana S, et al. Ingrowth of human mesenchymal stem cells into porous silk particle reinforced silk composite scaffolds: an in vitro study. Acta Biomater. 2011; 7:144–51. [PubMed: 20656075]

32. Grayson WL, Martens TP, Eng GM, Radisic M, Vunjak-Novakovic G. Biomimetic approach to tissue engineering. Semin Cell Dev Biol. 2009; 20:665–73. [PubMed: 19146967]

33. Mauney JR, Blumberg J, Pirun M, Volloch V, Vunjak-Novakovic G, Kaplan DL. Osteogenic differentiation of human bone marrow stromal cells on partially demineralized bone scaffolds in vitro. Tissue Eng. 2004; 10:81–92. [PubMed: 15009933]

34. Urist MR, DeLange RJ, Finerman GA. Bone cell differentiation and growth factors. Science. 1983; 220:680–6. [PubMed: 6403986]
35. Wang J, Glimcher MJ. Characterization of matrix-induced osteogenesis in rat calvarial bone defects: I. Differences in the cellular response to demineralized bone matrix implanted in calvarial defects and in subcutaneous sites. Calcif Tissue Int. 1999; 65:156–65. [PubMed: 10430651]
36. Zeltinger J, Sherwood JK, Graham DA, Mueller R, Griffith LG. Effect of pore size and void fraction on cellular adhesion, proliferation, and matrix deposition. Tissue Eng. 2001; 7:557–72. [PubMed: 11694190]
37. Akay G, Birch MA, Bokhari MA. Microcellular polyHIPE polymer supports osteoblast growth and bone formation in vitro. Biomaterials. 2004; 25:3991–4000. [PubMed: 15046889]
38. Akin FA, Zreiqat H, Jordan S, Wijesundara MB, Hanley L. Preparation and analysis of macroporous TiO2 films on Ti surfaces for bone-tissue implants. J Biomed Mater Res. 2001; 57:588–96. [PubMed: 11553890]
39. Bjerre L, Bunger C, Baatrup A, Kassem M, Mygind T. Flow perfusion culture of human mesenchymal stem cells on coralline hydroxyapatite scaffolds with various pore sizes. J Biomed Mater Res A. 2011; 97:251–63. [PubMed: 21442726]
40. Carlberg B, Axell MZ, Nannmark U, Liu J, Kuhn HG. Electrospun polyurethane scaffolds for proliferation and neuronal differentiation of human embryonic stem cells. Biomed Mater. 2009; 4:045004. [PubMed: 19567936]
41. Ouyang A, Ng R, Yang ST. Long-term culturing of undifferentiated embryonic stem cells in conditioned media and three-dimensional fibrous matrices without extracellular matrix coating. Stem Cells. 2007; 25:447–54. [PubMed: 17023515]
42. Karageorgiou V, Kaplan D. Porosity of 3D biomaterial scaffolds and osteogenesis. Biomaterials. 2005; 26:5474–91. [PubMed: 15860204]
43. Grayson WL, Bhumiratana S, Cannizzaro C, Chao PH, Lennon DP, Caplan AI, et al. Effects of initial seeding density and fluid perfusion rate on formation of tissue-engineered bone. Tissue Eng Part A. 2008; 14:1809–20. [PubMed: 18620487]
44. Grayson WL, Frohlich M, Yeager K, Bhumiratana S, Chan ME, Cannizzaro C, et al. Engineering anatomically shaped human bone grafts. Proc Natl Acad Sci U S A. 2010; 107:3299–304. [PubMed: 19820164]
45. Marolt D, Campos IM, Bhumiratana S, Koren A, Petridis P, Zhang G, et al. Engineering bone tissue from human embryonic stem cells. Proc Natl Acad Sci U S A. 2012
46. Washburn EW. Note on a method of determining the distribution of pore sizes in a porous material. Proc Natl Acad Sci U S A. 1921; 7:115–6. [PubMed: 16576588]
47. Rootare HMPC. Surface areas from mercury porosimetry measurements. J Phys Chem. 1967; 71:2733–36.
48. Liu XS, Sajda P, Saha PK, Wehrli FW, Guo XE. Quantification of the roles of trabecular microarchitecture and trabecular type in determining the elastic modulus of human trabecular bone. J Bone Miner Res. 2006; 21:1608–17. [PubMed: 16995816]
49. Zhang Y, Zhang M. Three-dimensional macroporous calcium phosphate bioceramics with nested chitosan sponges for load-bearing bone implants. J Biomed Mater Res. 2002; 61:1–8. [PubMed: 12001239]
50. Pittenger MF, Mackay AM, Beck SC, Jaiswal RK, Douglas R, Mosca JD, et al. Multilineage potential of adult human mesenchymal stem cells. Science. 1999; 284:143–7. [PubMed: 10102814]
51. Stains JP, Civitelli R. Cell-cell interactions in regulating osteogenesis and osteoblast function. Birth Defects Res C Embryo Today. 2005; 75:72–80. [PubMed: 15838921]
52. Karner E, Backesjo CM, Cedervall J, Sugars RV, Ahrlund-Richter L, Wendel M. Dynamics of gene expression during bone matrix formation in osteogenic cultures derived from human embryonic stem cells in vitro. Biochim Biophys Acta. 2009; 1790:110–8. [PubMed: 19007861]
53. Weber GF, Ashkar S, Glimcher MJ, Cantor H. Receptor-ligand interaction between CD44 and osteopontin (Eta-1). Science. 1996; 271:509–12. [PubMed: 8560266]

54. Zohar R, Suzuki N, Suzuki K, Arora P, Glogauer M, McCulloch CA, et al. Intracellular osteopontin is an integral component of the CD44-ERM complex involved in cell migration. J Cell Physiol. 2000; 184:118–30. [PubMed: 10825241]

55. Aubin JE, Liu F, Malaval L, Gupta AK. Osteoblast and chondroblast differentiation. Bone. 1995; 17:77S–83S. [PubMed: 8579903]

56. Stein GS, Lian JB. Molecular mechanisms mediating proliferation/differentiation interrelationships during progressive development of the osteoblast phenotype. Endocr Rev. 1993; 14:424–42. [PubMed: 8223340]

57. Anselme K. Osteoblast adhesion on biomaterials. Biomaterials. 2000; 21:667–81. [PubMed: 10711964]

58. Egusa H, Iida K, Kobayashi M, Lin TY, Zhu M, Zuk PA, et al. Downregulation of extracellular matrix-related gene clusters during osteogenic differentiation of human bone marrow- and adipose tissue-derived stromal cells. Tissue Eng. 2007; 13:2589–600. [PubMed: 17666000]

59. Tsigkou O, Jones JR, Polak JM, Stevens MM. Differentiation of fetal osteoblasts and formation of mineralized bone nodules by 45S5 Bioglass conditioned medium in the absence of osteogenic supplements. Biomaterials. 2009; 30:3542–50. [PubMed: 19339047]

60. Mauney JR, Jaquiery C, Volloch V, Heberer M, Martin I, Kaplan DL. In vitro and in vivo evaluation of differentially demineralized cancellous bone scaffolds combined with human bone marrow stromal cells for tissue engineering. Biomaterials. 2005; 26:3173–85. [PubMed: 15603812]

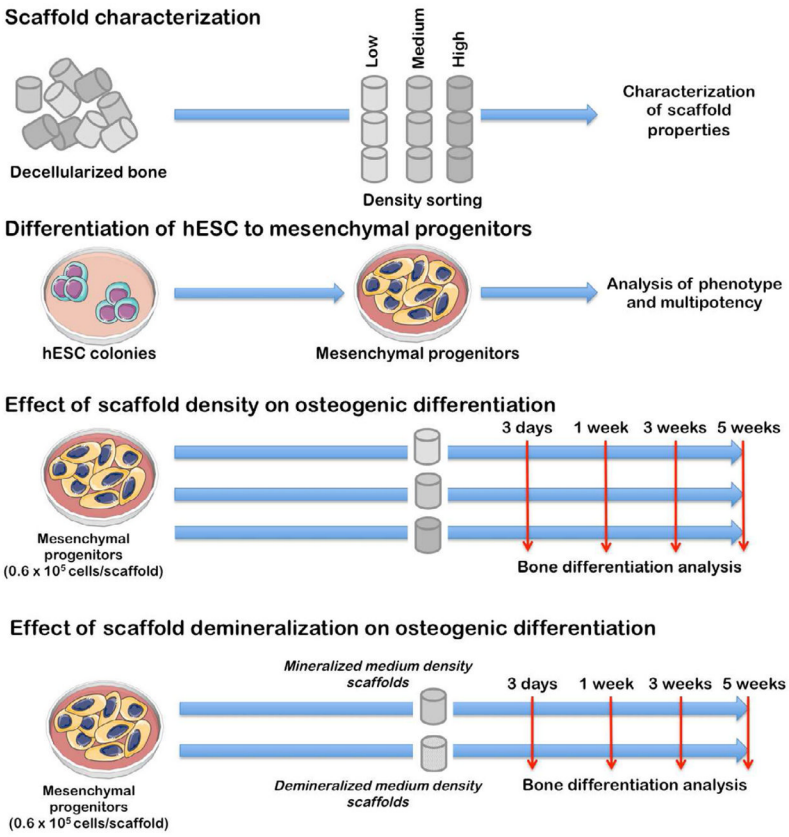

Figure 1. Experimental design

Scaffolds were sorted according to the mass density into three experimental groups (low, medium and high density) and their structural and mechanical properties were characterized. Medium density scaffolds were demineralized to assess the effect of matrix mineralization on osteogenesis. Human mesenchymal progenitors derived from hESC were characterized fir their phenotype and multipotency, seeded into scaffolds, and cultured for 5 weeks.

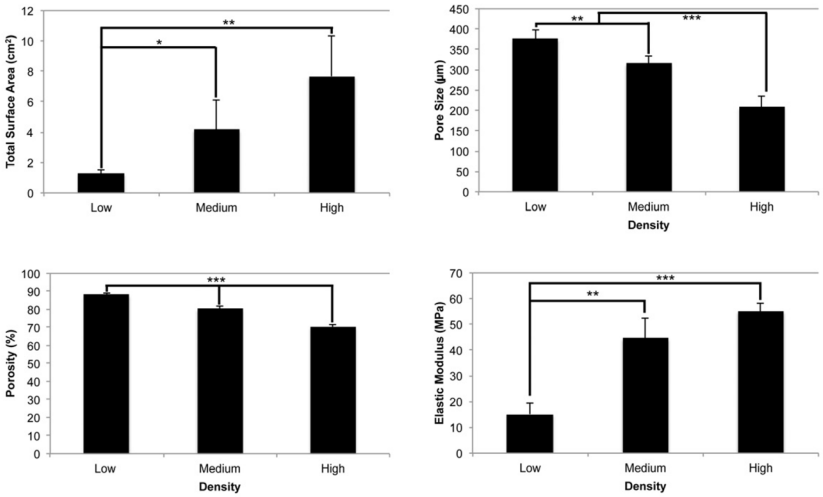

Figure 2. Scaffold characterization

Mercury porosimetry showed an increase in total surface area with increasing scaffold density (a), and a decrease in pore sizes with increasing scaffold density (b). μCT data indicated that bone scaffold porosity was decreasing with increasing scaffold density (c). Compressive elastic modulus was increasing with increasing scaffold density (d). Data represent average ± SD of n = 4 measurements, (*p<0.05; **p<0.01; ***p<0.001).

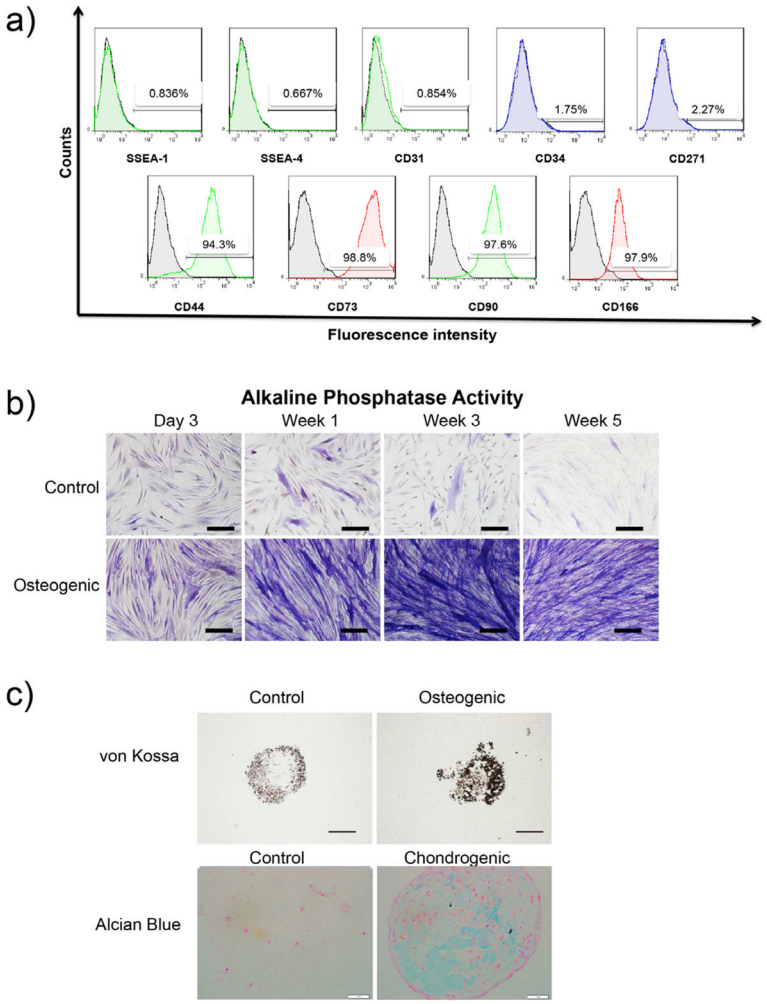

Figure 3. Mesenchymal progenitors

Flow cytometry data demonstrated lack of expression of hESC (SSEA-4), early differentiating cells (SSEA-1), endothelial cells (CD31), hematopoietic cells (CD34) and neural cells (CD261) specific markers. Positive expression of mesenchymal markers was detected in mesenchymal progenitors derived from hESC line H9 (a). Mesenchymal progenitor potential for osteogenesis was demonstrated by positive staining of alkaline phosphatase activity (purple) in monolayer cultures (scale bar: 100μm) (b). Pellet cultures indicated osteogenic and chondrogenic potential under adequate conditions, as shown by black von Kossa staining (matrix mineralization, scale bar: 500μm) and blue Alcian Blue staining (GAG) (scale bar: 250μm), respectively (c).

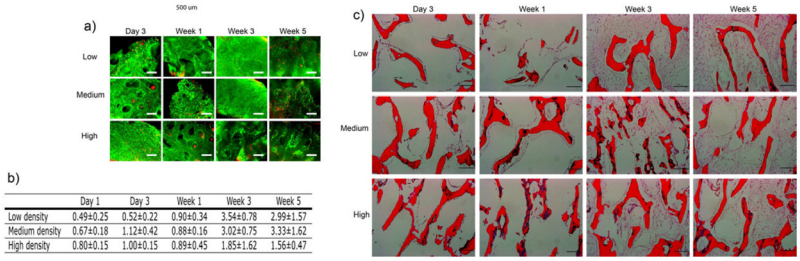

	Day 1	Day 3	Week 1	Week 3	Week 5
Low density	0.49±0.25	0.52±0.22	0.90±0.34	3.54±0.78	2.99±1.57
Medium density	0.67±0.18	1.12±0.42	0.88±0.16	3.02±0.75	3.33±1.62
High density	0.80±0.15	1.00±0.15	0.89±0.45	1.85±1.62	1.56±0.47

Figure 4. Survival and growth of mesenchymal progenitors in bone scaffolds

Live/dead assay of the constructs demonstrated uniform cell viability along the cultivation process (green indicates live cells, red indicates dead cells, scale bar: 500 μm) (a). DNA quantification showed an increase in cell numbers in medium- and high-density scaffolds when compared to low-density scaffolds (n=4) (b). Hematoxylin/eosin staining of construct sections showed uniform cell distribution by week 1. At week 5, the inner part of high-density scaffolds showed lack of cells in some areas. Scale bar: 200 μm (c).

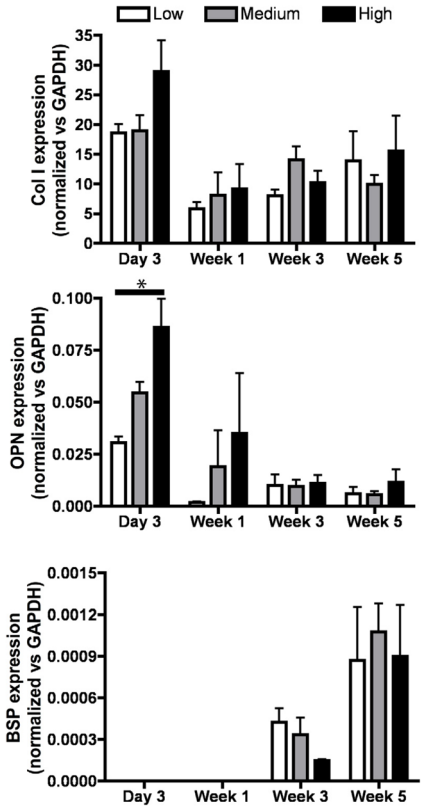

Figure 5. Osteogenic gene expression of mesenchymal progenitors in bone scaffolds

Expressions of type I collagen (Col I), osteopontin (OPN) and bone sialoprotein (BSP) were evaluated during the 5 weeks of culture under osteogenic conditions. All values were normalized to GAPDH. Data represent average ± SD (n=4, *p<0.05).

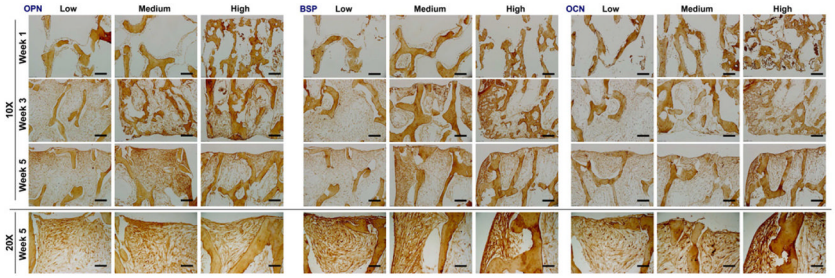

Figure 6. Deposition of new bone matrix in bone scaffolds

Bone matrix formation was confirmed by positive immunohistochemical staining of OPN, BSP and OCN (brown), with differences in distribution between the scaffold density groups (scale bars: 200 μm for 10x, 400 μm for 20x).

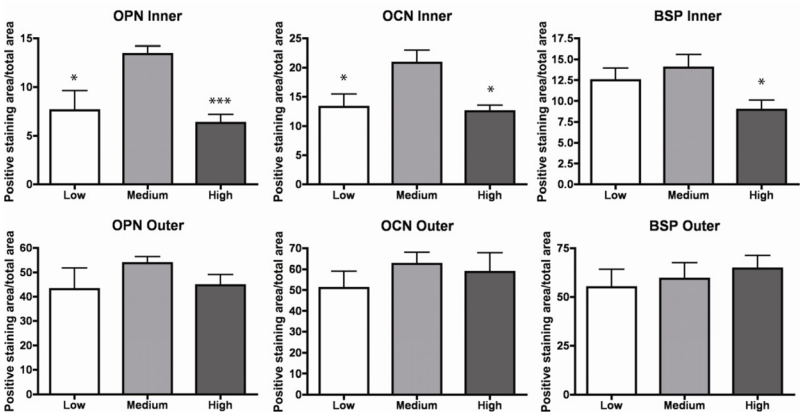

Figure 7. New bone matrix quantification

Construct areas staining positively for OPN, BSP and OCN were quantified by using Image J. Quantitative histomorphometric analyses indicated significantly higher area fraction stained positively in the inner part of medium-density scaffolds. Data represent average ± SD for n=4 (*p<0.05; **p<0.01; ***p<0.001).

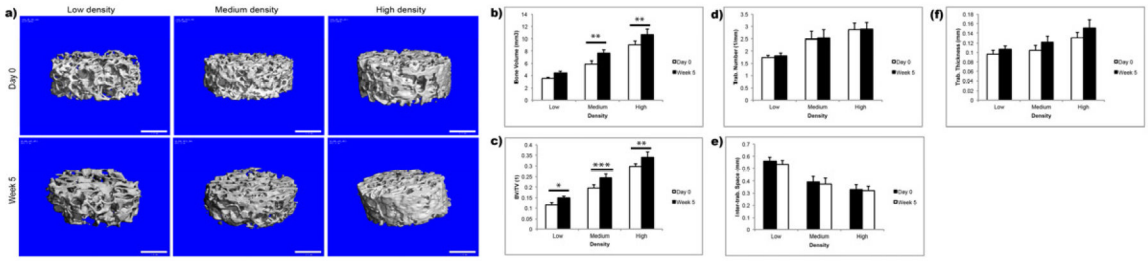

Figure 8. Mineralized tissue formation in bone scaffols

Reconstructed 3D μCT images of the engineered bone before and after 5 weeks of culture (scale bar: 1 mm) (a). Bone volume (BV) (b), bone volume to tissue volume fraction (BV/TV) (c), trabecular number (Tb.N.) (d), intertrabecular space (Tb.Sp.) (e), and trabecular thickness (Tb.Th.) (f) were determined by μCT analysis, and indicated bone maturation during *in vitro* culture. Data represent average ± SD, n=4 (*p<0.05; **p<0.01; ***p<0.001).

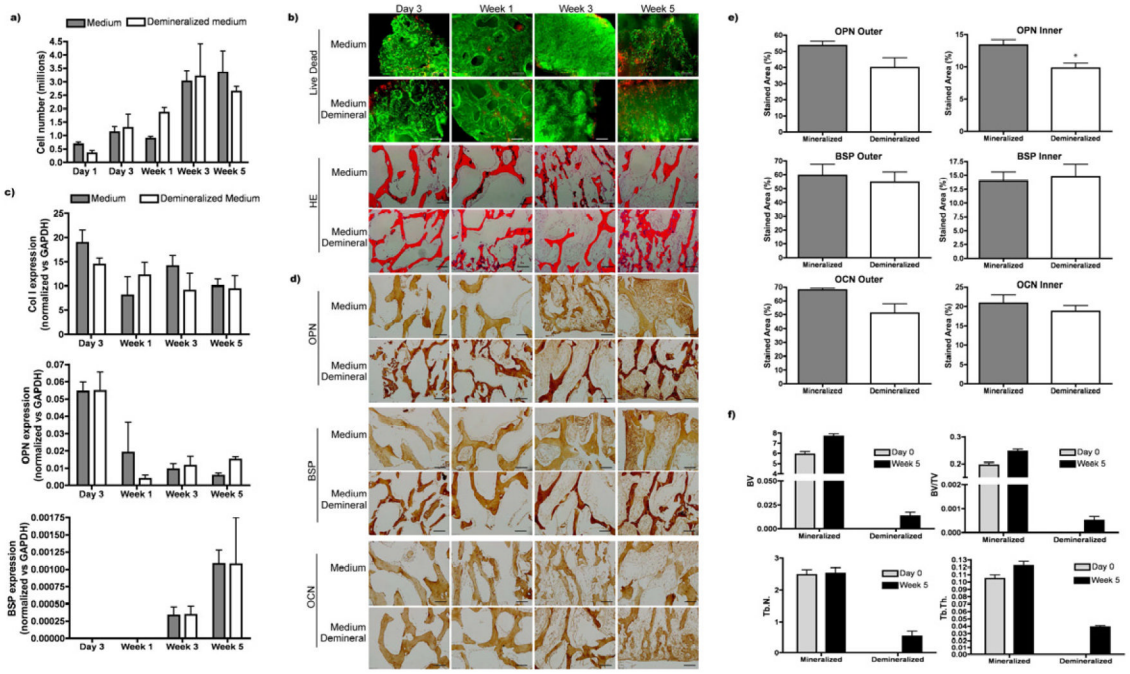

Figure 9. Effect of demineralization on osteogenesis in medium density scaffolds

Mesenchymal progenitors were cultured for 5 weeks in demineralized medium-density scaffolds. DNA quantification (a), cell viability and cell distribution (b) did not show differences between the native and demineralized groups. Gene expression followed the characteristic bone formation pattern (c). Immunohistochemistry demonstrated comparable accumulation of bone specific proteins (scale bar: 200 μm) (d, e). In contrast, mCT demonstrated markedly higher mineralized tissue formation in native compared to demineralized bone scaffolds of medium density (f). Data represent average ± SD, n=4.